Unexpected superconductivity at nanoscale junctions made on the topological crystalline insulator $Pb_{0.6}Sn_{0.4}Te$

Shekhar Das[1], Leena Aggarwal[1], Subhajit Roychowdhury[2], Mohammad Aslam[1], Sirshendu Gayen[1], Kanishka Biswas[2],[*] and Goutam Sheet[1][†]

[1]*Department of Physical Sciences, Indian Institute of Science Education and Research Mohali, Sector 81, S. A. S. Nagar, Manauli, PO: 140306, India and*

[2]*New Chemistry Unit, Jawaharlal Nehru Center for Advanced Scientific Research, Jakkur, P.O., Bangalore 560064, India*

Abstract

Discovery of exotic phases of matter from the topologically non-trivial systems not only makes the research on topological materials more interesting but also enriches our understanding of the fascinating physics of such materials. $Pb_{0.6}Sn_{0.4}Te$ was recently shown to be a topological crystalline insulator. Here we show that by forming a mesoscopic point-contact using a normal non-superconducting elemental metal on the surface of $Pb_{0.6}Sn_{0.4}Te$ a novel superconducting phase is created locally in a confined region under the point-contact. This happens while the bulk of the sample remains to be non-superconducting and the superconducting phase emerges as a nano-droplet under the point-contact. The superconducting phase shows a high transition temperature T_c that varies for different point-contacts and falls in a range between 3.7 K and 6.5 K. Therefore, this Letter presents the discovery of a new superconducting phase on the surface of a topological crystalline insulator and the discovery is expected to shed light on the mechanism of induced superconductivity in topologically non-trivial systems in general.

---

[*]Electronic address: kanishka@jncasr.ac.in

[†]Electronic address: goutam@iisermohali.ac.in

It is known that perturbations like magnetic dopant, structural distortion, mechanical strain and disorder etc. can be used to realize novel phases of matter out of the topological insulators (TIs)[1–6] and the topological crystalline insulators (TCIs)[7–16]. Based on these ideas, enormous amount of effort has been invested to create exotic superconducting phases from TIs[3] and TCIs[7,8,17] as the superconductors emerging from topologically non-trivial systems may show topological superconductivity and eventually may lead to the observation of Majorana modes in condensed matter systems[18–20]. Among the potential candidates for topological superconductors[4,8], Cu intercalated Bi_2Se_3[21–25], derived from the topological insulator Bi_2Se_3 has been investigated most widely. It is believed that the "glue" for Cooper pairing in this system is facilitated by the strong spin-orbit coupling of Bi_2Se_3. Within this idea, an electron's spin is locked to the orbital component and the momentum of the electron. Consequently, a short-ranged and spin-independent bare interaction in Cu intercalated Bi_2Se_3 is spontaneously converted to a spin-dependent and momentum dependent effective interaction between the Bloch electrons thereby leading to superconductivity.[21]

TCIs are fundamentally different from TIs (e.g. Bi_2Te_3, Bi_2Se_3) in terms of the protection mechanism of their surface states. TI surface states are protected by time reversal symmetry, while TCI surface states are protected by crystal symmetry[9,12,26,27]. It is also known that the TCI surface states are more tunable than that of TIs by perturbations[8]. Recently, the solid solution composition $Pb_{0.6}Sn_{0.4}Te$ derived from PbTe ($E_g \sim 0.29$ eV) and SnTe ($E_g \sim 0.18$ eV, inverted gap) has created new sensation as a new TCI as confirmed by angle-resolved photoemission spectroscopy (ARPES)[26]. Here we show that $Pb_{0.6}Sn_{0.4}Te$ shows superconductivity in a confined dimension when a mesoscopic point-contact made up of an elemental metal is formed on the surface of $Pb_{0.6}Sn_{0.4}Te$. The local superconducting phase shows a high critical temperature T_c that is contact-dependent and varies between 3.7 K and 6.5 K. Further theoretical studies will be required to understand the microscopic origin of the new phase.

In the inset of Figure 1 (a) we demonstrate a schematic diagram describing how the mesoscopic point contacts between the sharp tips of elemental metals and $Pb_{0.6}Sn_{0.4}Te$ were formed in-situ at low temperatures. The current and voltage leads are also shown. From the picture it is clear that the measurement is done in a pseudo four-probe geometry. A lock-in based modulation technique was employed to directly measure the differential conductance dI/dV of the point-contacts as a function of an applied DC bias V. The
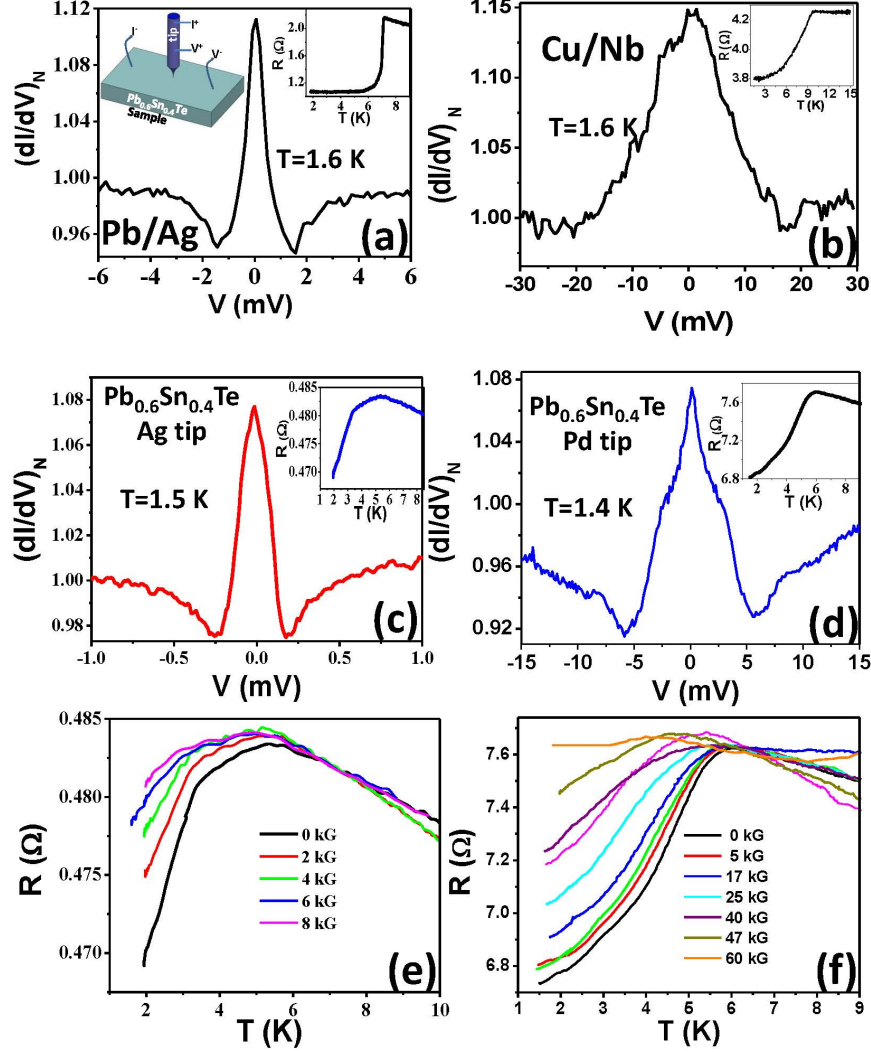
Figure 1: **Evidence of superconductivity in Pb$_{0.6}$Sn$_{0.4}$Te point-contacts.** (a) A normalized dI/dV spectrum between Ag and Pb, a conventional superconductor. inset: A schematic diagram showing the point contact on Pb$_{0.6}$Sn$_{0.4}$Te with measuring electrodes (left) and $R - T$ data showing superconducting transition at 7.1 K, the T_c of Pb (right). (b) A normalized dI/dV spectrum between a conventional superconductor Nb and Cu. inset: $R - T$ data showing superconducting transition at 9.4 K, the T_c of Nb (c) A normalized dI/dV spectrum for a point-contact on Pb$_{0.6}$Sn$_{0.4}$Te with an Ag tip. *inset*: $R - T$ data showing superconducting transition at 5.4 K. (d) A normalized dI/dV spectrum for a point-contact between Pb$_{0.6}$Sn$_{0.4}$Te and a Pd tip. *inset*: $R - T$ showing superconducting transition at 6 K. Magnetic field dependence of $R - T$ for point-contacts with (e) an Ag tip and (f) a Pd tip.

resistance R_{PC} of a mesoscopic point-contact between two materials is given by Wexler's

formula[28]: $R_{PC} = \frac{2h/e^2}{(ak_F)^2} + \Gamma(l/a)\frac{\rho(T)}{2a}$, where h is Planck's constant, e is the charge of a single electron, a is the contact diameter, $\Gamma(l/a)$ is a slowly varying function of the order of unity, ρ is the bulk resistivity of the material and T is the effective temperature at the point-contact. The first term is known as ballistic or Sharvin's resistance (R_S) and it is independent of the bulk resistivity of the materials forming the point-contact and independent of temperature. The second term is called the Maxwell's resistance (R_M) which depends directly on the resistivity of the materials. The above equation suggests when the contact diameter is small compared to electronic mean free path (ballistic regime) R_S dominates and when the contact diameter is large (thermal regime), R_M contributes most to the total contact resistance. Therefore resistive transitions lead to non-linearities in the $I-V$ characteristics corresponding to R_M of point-contacts. Clearly, from Wexler's formula given above, such non-linearities associated with change in ρ are pronounced when a (contact diameter) is large and the point-contacts are in the so-called thermal regime of mesoscopic transport.

One example of a sharp resistive transition is the superconducting transition. This resistive transition can take place when the current flowing through a superconductor exceeds the critical current (I_c). If we consider the $I-V$ characteristic of a superconductor, we observe that below I_c the voltage remains zero and above I_c the superconductor slowly becomes resistive thereby making the voltage drop across it finite[29]. When such a $I-V$ curve is differentiated, two sharp dips are expected to appear in the dI/dV vs. V spectra[30]. Therefore, two sharp dips symmetric about $V = 0$ in dI/dV spectra from non-ballistic point-contacts (a large) might indicate the existence of superconductivity at the point-contacts. In addition, since below I_c the heating effect on a thermal regime point-contact is minimized (due to the superconducting transition of one of the electrodes), a sharp increase in zero-bias conductance is also expected[30].

As a test case, in Figure 1(a) and Figure 1(b) we show two dI/dV spectra for point-contacts involving the conventional superconductors lead (Pb) and Nb respectively. Two sharp dips in conductance that are symmetric about $V = 0$ is observed on the Pb/Ag point-contact spectrum due to the critical current of the point-contact. $R-T$ of the point-contact shows a sharp change corresponding to the superconducting transition of Pb at 7.1 K as shown in the inset of Figure 1(a). As it is seen in Figure 1(b), sometimes the critical current driven conductance dips may not appear to be prominent.

The dI/dV spectra obtained on Ag/Pb$_{0.6}$Sn$_{0.4}$Te and Pd/Pb$_{0.6}$Sn$_{0.4}$Te point-contacts are

shown in Figure 1(c) and Figure 1(d) respectively. The spectra show two sharp conductance dips symmetric about $V = 0$ as well as a sharp conductance peak at $V = 0$. This is strikingly similar to the data obtained on Pb/Ag point-contacts (Figure 1(b)) where the conductance dips appear due to the critical current of the superconductor and the zero-bias peak appears due to the transition of the superconducting part of the point-contact to a zero-resistance state.[30] In addition, as shown in the insets of Figure 1(c) and Figure 1(d), the superconducting transition for the two point-contacts on $Pb_{0.6}Sn_{0.4}Te$ are clearly seen at temperatures 5.5 K and 6.3 K respectively. We have obtained such results on more than 50 point-contacts on $Pb_{0.6}Sn_{0.4}Te$ with different elemental metallic tips. Therefore, it is concluded that the metallic point-contacts on $Pb_{0.6}Sn_{0.4}Te$ are superconducting.

In order to establish the observation of superconductivity on the metallic point-contacts on $Pb_{0.6}Sn_{0.4}Te$ more firmly it is necessary and sufficient to confirm the validity of the following three key facts about superconducting point-contacts for the point-contacts made on $Pb_{0.6}Sn_{0.4}Te$: (i) The superconducting transition as observed in the $R - T$ data shows systematic magnetic field dependence. (ii) The dI/dV spectra show systematic temperature dependence and the spectral features smear out at T_c and (iii) The dI/dV spectra show systematic magnetic field dependence and the spectral features disappear at H_c of a given point-contact. In the following sections we will demonstrate the validity of all the three points mentioned above for the point-contacts made on $Pb_{0.6}Sn_{0.4}Te$.

(i) $R - T$ **data shows systematic magnetic field dependence:** The magnetic field dependence of the $R - T$ data is shown for two point-contacts on $Pb_{0.6}Sn_{0.4}Te$, one with a Ag tip (Figure 1(e)) and the other one with a Pd tip (Figure 1(f)). The $R - T$ curves evolve smoothly with magnetic field. As the magnetic field is increased, the transition temperature systematically goes down.

It should be noted here that the over-all resistance of a bulk superconductor can be measured to be zero in a four-probe geometry. However, for a superconducting point-contact[31], the contact resistance does not approach zero. This is due to (a) the existence of a non-superconducting component of the point-contact (in this case, a normal metal), (b) existence of a small temperature independent ballistic resistance even when the contacts are far from the ballistic regime and (c) the intrinsic mismatch of the Fermi-velocities in the two electrodes forming the metallic point-contact. Consequently, the existence of superconductivity in a confined geometry under a metallic point-contact cannot be characterized by a di-

rectly measurable zero-resistance. This is further clear from the $R - T$ data obtained from point-contacts on superconducting Pb (inset of Figure 1(a)).

(ii) The dI/dV spectra show systematic temperature dependence and the spectral features smear out at T_c: In Figure 2(a) we show the temperature dependence of one of the representative dI/dV spectrum obtained on Pd/Pb$_{0.6}$Sn$_{0.4}$Te point-contacts. From the visual inspection alone it is clear that the spectrum smoothly evolves with increasing magnetic field and the spectral features disappear around 6 K, which is the critical temperature as obtained from the transport data at zero magnetic field.
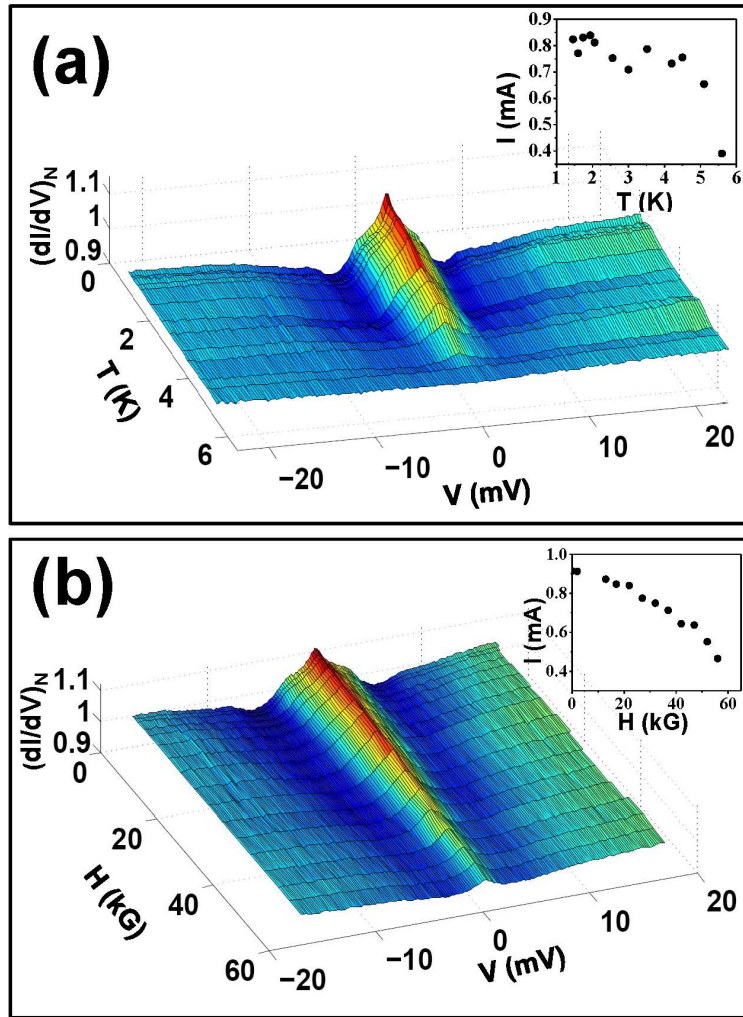

Figure 2: **Temperature and magnetic field dependence:** (a) Evolution of the point-contact spectrum between Pb$_{0.6}$Sn$_{0.4}$Te and Pd point-contacts with temperature. *inset:* Temperature dependence of I_c. (b) Evolution of the point-contact spectrum with magnetic field. *inset*: Magnetic field dependence of I_c.

The position of the conductance dips observed in dI/dV gives the estimate of the critical current. This is nothing but the ratio of the magnitude of the DC voltage (V) for which the conductance dips appear and the value of the normal state resistance. The critical current thus measured is plotted as a function of temperature in the inset of Figure 2(a). As expected for superconducting point-contacts, the critical current decreases with increasing temperature. Using Wexler's formula and the measured normal state resistance it is also possible to estimate the diameter of the point-contact which is found to be 50 nm in this case. Using this length scale the critical current density is estimated to be of the order of 10^6 A/cm^2 which is reasonable for superconducting point-contacts.

(iii) The dI/dV spectra show systematic magnetic field dependence and the spectral features disappear at H_c of a given point-contact: In order to inspect the validity of this point we show the magnetic field dependence of an Pd/Pb$_{0.6}$Sn$_{0.4}$Te point-contact spectrum in Figure 2(b). As expected for superconducting point-contacts, the spectrum shows a monotonic decrease in the spectral features with increasing magnetic field. Beyond a critical magnetic field of 5 T, the spectrum becomes featureless and that is the critical magnetic field for the superconducting point-contact. The magnetic field dependence of the critical current is demonstrated in the inset of Figure 2(b).

Therefore, we have confirmed the existence of a superconducting phase in Pd/Pb$_{0.6}$Sn$_{0.4}$Te point-contacts.

Having confirmed the existence of a superconducting phase it is now important to investigate the nature of superconductivity in the new phase. In Figure 3(a) and Figure 3(b) we show the $H - T$ phase diagrams constructed for the superconducting phases appearing at Ag/Pb$_{0.6}$Sn$_{0.4}$Te and Pd/Pb$_{0.6}$Sn$_{0.4}$Te point-contacts respectively. In both cases the experimentally obtained $H - T$ curves, within the range of the measurement errors, are seen to fall on the empirically expected $H - T$ phase curves for conventional superconductors.

Since the superconducting phase has been derived from a topologically non-trivial system the possibility of a p-wave symmetry of the superconducting order parameter must be addressed too.[19] Since for a p-wave symmetry, the time-reversal symmetry is naturally broken, the proximity of a spin-polarized Fermi surface should favour superconductivity. This is in contrast to the conventional BCS-type of superconductors where the proximity of a ferromagnet competes with and suppresses the superconducting order. We report our experimental results on Pb$_{0.6}$Sn$_{0.4}$Te with two metallic ferromagnetic tips Co and Ni in Figure
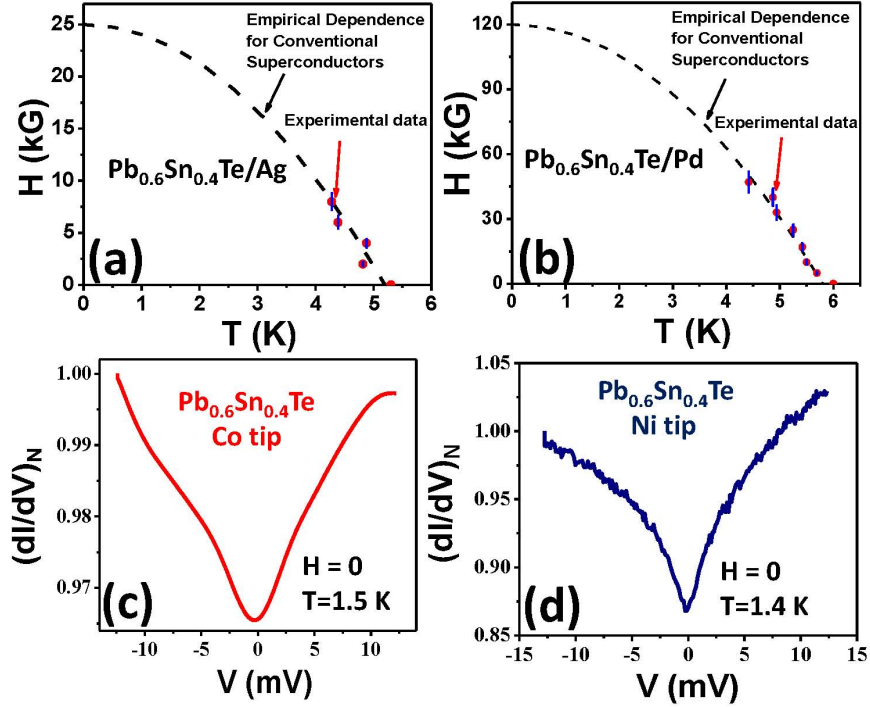
Figure 3: $H - T$ phase diagram obtained for (a) Ag and (b) Pd point-contacts on $Pb_{0.6}Sn_{0.4}Te$. These data have been extracted from Figure 1(e) and Figure 1(f) respectively (Error bars are also shown). The dotted lines show the empirical dependence expected for conventional superconductors. Representative point-contact spectrum (c) with a cobalt tip and (d) with a nickel tip on $Pb_{0.6}Sn_{0.4}Te$.

3(c) and Figure 3(d) respectively. As it is seen, with the ferromagnetic tips, the dI/dV spectrum shows a sharp dip at zero-bias indicating the presence of a gap structure in the density of states. However, no signature of Andreev reflection or critical current dominated effects could be found. At this point the change in the over all shape of the spectra in the proximity of a spin-polarized metal is not understood and this calls for detailed theoretical investigation of spin-polarized transport at mesoscopic interfaces on a topological crystalline insulator. On the other hand the over all shape of the point-contact spectra presented here and their magnetic field dependence show remarkable similarities with the spectra earlier obtained on Cu-intercalated Bi_2Se_3.[4] In that case the sharp zero-bias conductance peak and the unique magnetic field dependence of the same was attributed to the existence of Majorana bound states in Cu-intercalated Bi_2Se_3.[4]

In this context it is also important to discuss other possible origins of a ZBCP other

than superconductivity. In the past it was shown that in semiconducting quantum dot systems a ZBCP might originate due to Kondo effect. However, in such cases the peak is expected to show logarithmic temperature dependence and a splitting with magnetic field.[32,33] Another possibility is a modulation of the density of states at zero-bias due to effects other than superconductivity.[11,34,35] However, such effects are not expected to show the unique temperature and magnetic field dependence that we observe here. Furthermore, the fact that for certain point contacts we also observe clear signature of Andreev reflection also confirms that the possibilities other than superconductivity can be ruled out for the emergence of the ZBCP in our case.

In principle, the idea of the superconducting order parameter here could be confirmed by measuring the superconducting energy gap through Andreev reflection spectroscopy as a function of temperature with non-ferromagnetic tips. We have attempted to obtain Andreev reflection dominated spectra in the ballistic limit of transport. For such measurements it is required to make the point-contact size smaller than the mean free path. For our $Pb_{0.6}Sn_{0.4}Te$ samples, the pure ballistic regime could not be achieved possibly due to intrinsic disorder existing in the samples. However, as shown in the supplementary material (Figure S11), we obtained strong signature of Andreev reflection (please note the double peak structure in dI/dV symmetric about $V = 0$) in the last four spectra in Figure S11. These spectra also have strong non-ballistic contribution (confirmed by the sharp dips in dI/dV) and consequently could not be used for energy resolved spectroscopy.

Since the topological materials in general have low carrier density the observation of a high critical temperature of 6.5 K is intriguing. As per existing theories the expected transition temperature in such systems is very low and mostly in the milikelvin regime. Furthermore, the existence of a superconducting phase only in a confined geometry with such a high critical temperature on the surface of a topological crystalline insulator is even more intriguing. In this context it may be noted that earlier a superconducting phase was shown to exist at the mesoscopic point-contacts formed on the three dimensional Dirac semi-metal Cd_3As_2[36].

Stoichiometrically pure $Pb_{0.6}Sn_{0.4}Te$ samples were used for all the measurements presented here. Since Pb and Sn are also known to superconduct, detailed elemental analysis have been performed to rule out the possibility of obtaining a superconducting signal from local clustering of Pb or Sn.[37] Moreover, the transition temperature and the critical fields

that we measure are significantly different from that expected for Pb or Sn. It should also be noted that the samples used for the presented measurement were polycrystalline in nature. However, as shown in the supplementary material (Figure S5), the grain size of the polycrystals are large ($\sim 100\mu$). Therefore, majority of the times the point-contact was established on a single crystallite. Since we have obtained the signature of superconductivity at all points on the polycrystalline samples with large crystallites (Please see Figure S11 in the supplementary material), it is reasonable to conclude that all the crystal facets of $Pb_{0.6}Sn_{0.4}Te$ show superconductivity under metallic point-contacts.

In conclusion, we have provided spectroscopic indication of the emergence of a novel superconducting phase at the mesoscopic point-contacts on the topological crystalline insulator $Pb_{0.6}Sn_{0.4}Te$. The discovery adds an important new candidate in the class of superconductors derived from topologically non-trivial systems. The results will be extremely helpful in understanding the origin of unexpected superconductivity with relatively high critical temperatures in topological materials in general.

[1] Peng H. *et al.*, *Phys. Rev. B.*, **88** (2013) 024515.

[2] Kirzhner T., Lahoud E., Chaska K. B., Salman Z. and Kanigel A., *Phys. Rev. B.,* **86** 2012 064517.

[3] Sasaki S. *et al.*, *Phys. Rev. Lett.*, **107** (2011) 217001.

[4] Hor Y. S., *et al.*, *Phys. Rev. Lett.*, **104** (2010) 057001.

[5] Hasan M. Z. and Kane C. L., *Rev. Mod. Phys.*, **82** (2010) 3045.

[6] Qi Xiao-Liang and Zhang Shon-Cheng, *Rev. Mod. Phys.*, **83** (2011) 1057.

[7] Sato T. *et al.*, *Phys. Rev. Lett.*, 110 (2013) 206804.

[8] Ando Y. and Fu L., *Cond. Mat. Phys.*, **6** (2015) 361.

[9] Fu L., *Phys. Rev. Lett.*, **106** (2011) 106802.

[10] Liu J. *et al.*, *Nat. Mater.*, **13** (2014) 178.

[11] Zeljkovic I. *et al.*, *Nature Materials*, **14** (2015) 318-324.

[12] Liang T. *et al.*, *Nature Communications*, **4** (2013) 2696.

[13] Mitrofanov K. V. *et al.*, *J. Phys.: Condens. Matter.*, **26** (2014) 475502.

[14] Zeljkovic I. *et al.*, *Nature Physics*, **10** (2014) 572-577.

[15] Okada Y. *et al.*, *Science*, **341** (2013) 1496.

[16] Erickson A. S., Chu J. H. M., Toney F., Geballe T. H. and Fisher I. R., *Phys. Rev. B.*, **79** (2009) 024520.

[17] Balakrishnan G., Bawden L., Cavendish S. and Lees M. R., *Phys. Rev. B.*, **87** (2013) 140507(R).

[18] Leijnse Martin, Flensberg Karsten, *Semicond. Sci. Technol.*, **27** (2012) 124003.

[19] Fu L. and Kane C. L., *Phys. Rev. Lett.*, **100** (2008) 096407.

[20] Beenakker C. W. J., *Annu. Rev. Con. Mat. Phys.*, **4** (2013) 113-136.

[21] Wray L. Andrew, *et al.*, *Nature Physics,* **6** (2010) 855-859.

[22] Hor Y. S., Checkelsky J. G., Qu D., Ong N. P. and Cava R. J., *J. Phys. Chem. Solids*, **72** (2011) 572-576.

[23] Kriener M., Segawa Kouji, Ren Zhi, Sasaki Satoshi, Wada Shohei, Kuwabata Susumu and Ando Yoichi, *Phys. Rev. B.*, **84** (2011) 054513.

[24] Kriener M, Segawa Kouji, Ren Zhi, Sasaki Satoshi and Ando Yoichi, *Phys. Rev. Lett.*, **106** (2011) 127004.

[25] Bay T. V., Naka T., Huang Y. K., Luigjes H., Golden M. S. and Visser de A., *Phys. Rev. Lett.*, **108** (2012) 057001.

[26] Xu Su-Yang *et al.*, *Nature Communications,* **3** (2012) 1192.

[27] Hsieh h. T., Lin H., Liu J., Duan W., Bansil A. and Fu L., *Nature Communications,* **3** (2012) 982.

[28] Wexler A., *Proc. Phys. Sov.*, **89** (1966) 927.

[29] Tinkham M., Introduction to Superconductivity, Dover, Second Edition (2004).

[30] Sheet Goutam, Mukhopadhyay S. and Raychaudhuri P., *Phys. Rev. B.*, **69** (2004) 134507.

[31] Naidyuk Y. G. and Yanson K. I., Point-Contact Spectroscopy, Springer (2005).

[32] Cho Sungjae, Zhong Ruidan, Schneeloch John A., Gu Genda, and Mason Nadya, *Sci. Rep.,* **6** (2016) 21767.

[33] Wiel W. G. van der, *et al., Science,* **289** (2000) 2105

[34] Druppel Matthias, Kruger Peter and Rohlfing Michael, *Phys. Rev. B.,* **90** 2014 155312.

[35] Venema L. C., Janssen J. W., Buitelaar M. R., Wildoer J. W. G., Lemay S. G., Kouwenhoven L. P. and Dekker C., *Phys. Rev. B.,* **62** 2000 5238.

[36] Aggarwal Leena, Gaurav Abhishek, Thakur Gohil S., Haque Zeba, Ganguli Ashok K., Sheet Goutam, *Nature Materials.* **15** (2016) 32-37.

[37] See online supplementary materials.

Supplemental material for "Unexpected superconductivity at nanoscale junctions made on the topological crystalline insulator Pb$_{0.6}$Sn$_{0.4}$Te"

(I) **Reagents:** Tin (Sn, Alfa Aesar 99.99+ %), tellurium (Te, Alfa Aesar 99.999+ %) and lead (Pb, Alfa Aesar 99.99+ %) were used for synthesis without further purification.

(II) <u>Material synthesis:</u> High quality ingots ($\sim$1 g) of Pb$_{0.6}$Sn$_{0.4}$Te was synthesized by mixing appropriate ratios of high-purity elemental Sn, Pb and Te in quartz tube. The tube was sealed under vacuum (10^{-5} Torr) and slowly heated to 723 K over 12 hrs, then heated up to 1323 K in 5 hrs, soaked for 5 hrs, and cooled down to 1023 K over 2 hrs and soaked for 4 hrs, then slowly cool down to room temperature over a period of 18 hrs.

(III) <u>Structural and chemical analysis of materials:</u>

Powder X-ray diffraction: Powder X-ray diffraction for finely grinded sample was recorded using a Cu K$_\alpha$(= 1.5406 A^o) radiation on a Bruker D8 diffractometer. Powder X-ray diffraction (PXRD) pattern of as synthesized polycrystalline $Pb_{0.6}Sn_{0.4}Te$ could be index based on cubic PbTe structure (space group, Fm-3m). PXRD of $Pb_{0.6}Sn_{0.4}Te$ are in well match with simulated PXRD pattern from the single crystal data of closest composition $Pb_{0.7}Sn_{0.3}Te$ (Figure S1a, supporting information). We have further compared PXRD data of $Pb_{0.6}Sn_{0.4}Te$ with pristine $PbTe$ and $SnTe$ in Figure S1b and 1c in supporting information. Highest intensity (200) peak of $Pb_{0.6}Sn_{0.4}Te$ lies in between that of $PbTe$ and $SnTe$ (Figure 1c in supporting information), which confirms complete solid solution formation $Pb_{0.6}Sn_{0.4}Te$, thus no phase separation occurs.
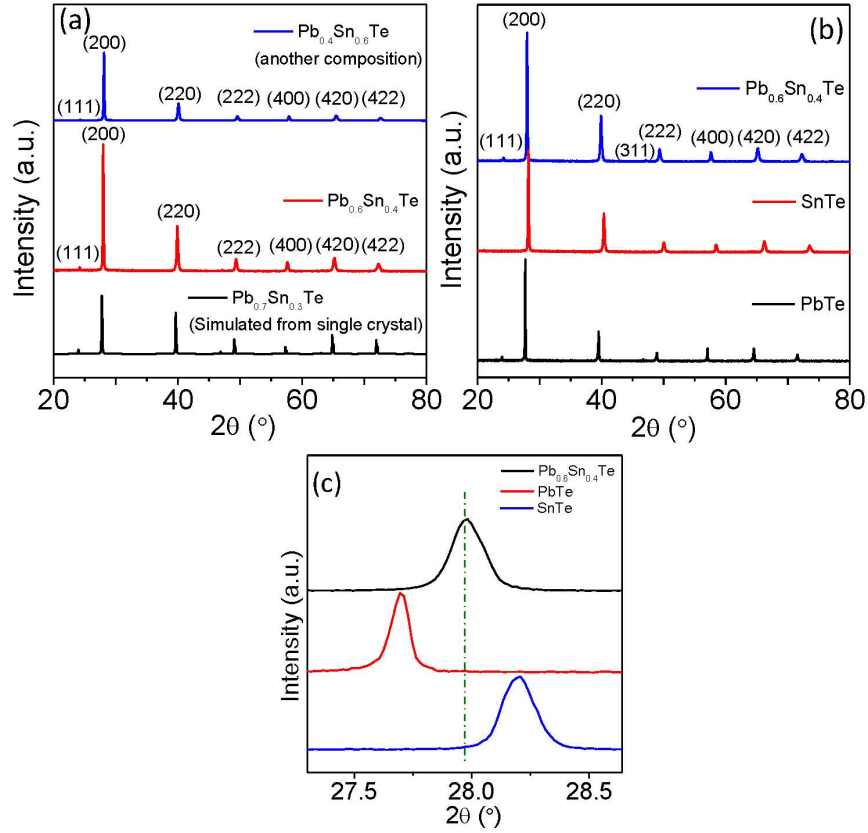
Figure S1: (a) Powder X-ray diffraction patterns of $Pb_{0.6}Sn_{0.4}Te$ and $Pb_{0.4}Sn_{0.6}Te$ samples. Simulated PXRD from the single crystal of $Pb_{0.7}Sn_{0.3}Te$ are given for comparison. (b) Powder X-ray diffraction patterns of $Pb_{0.6}Sn_{0.4}Te$, $PbTe$ and $SnTe$. (c) Zoomed XRD patterns from 27.2 to 28.6 degree for Figure (b).
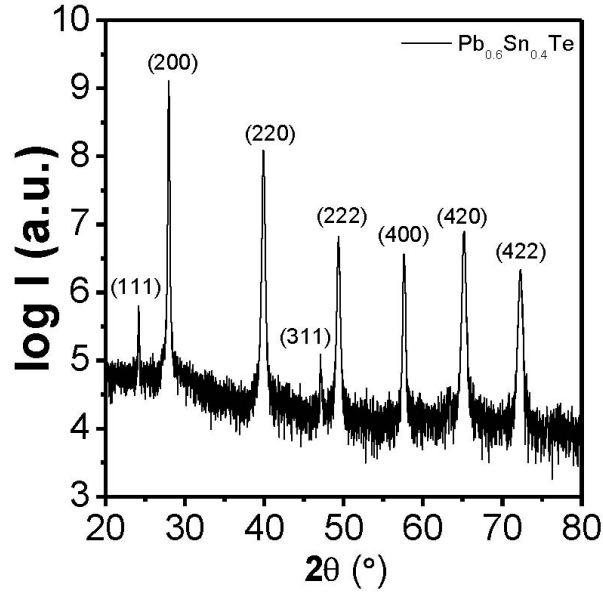
Figure S2: (a) Powder X-ray diffraction patterns of $Pb_{0.6}Sn_{0.4}Te$ in logarithmic scale.

X-ray photoelectron spectroscopy: XPS measurement has been performed with $MgK_{\alpha}(1253.6eV)$ X-ray source with a relative composition detection better than 0.1% on an Omicron Nano-technology spectrometer. The coordination number of Te is six and Te is bonded to Sn as well as Pb in $Pb_{0.6}Sn_{0.4}Te$. Thus, Te experiences different chemical environment from Pb and Sn. Difference of electronegativity between Sn and Te is small compared to that of Pb and Te. Covalent nature of $SnTe$ is higher than $PbTe$. Thus, Te bonded with Sn has higher binding energy than that of bonded with Pb. Therefore, Te 3d5/2 and 3d3/2 peaks are seen to be spitted in two peaks.
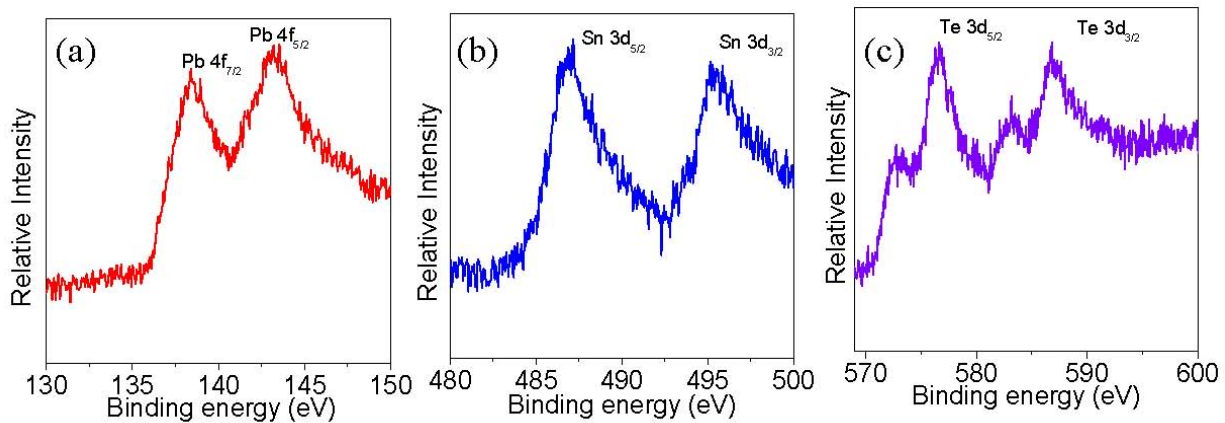
Figure S3: XPS spectra of $Pb_{0.6}Sn_{0.4}Te$. (a) Pb (2+) 4f, (b) Sn (2+) 3d, and (c) Te (2-) 3d spectra.

Energy Dispersive X-ray analysis: EDAX compositional analysis was performed during FESEM imaging. Errors in the determination in compositions of $Pb_{0.6}Sn_{0.4}Te$ in EDAX measurements is nearly 5 %.
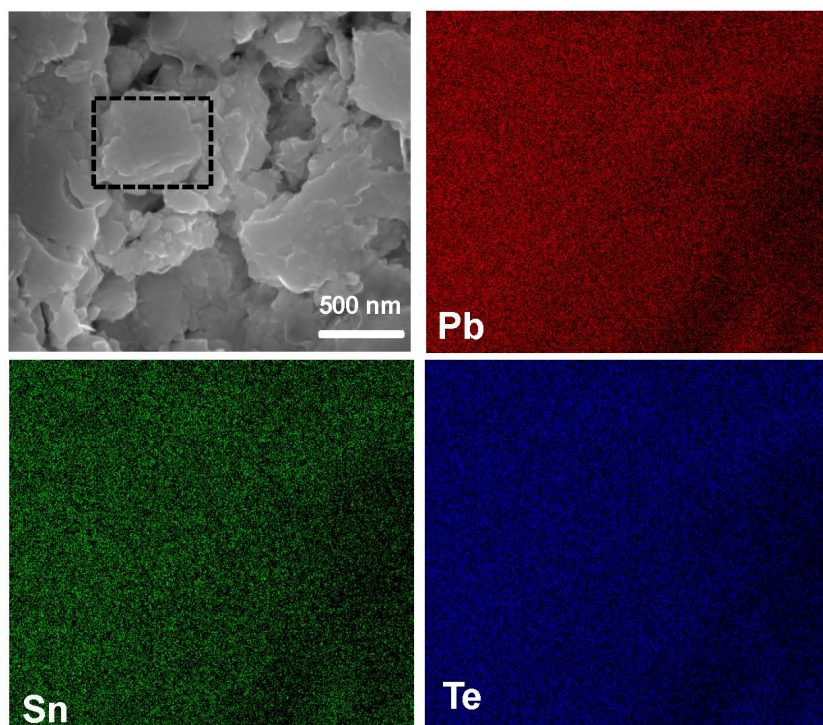

Figure S4: (a) EDAX color mapping of freshly cleaved surface of $Pb_{0.6}Sn_{0.4}Te$ showing the presence of all elements (Pb, Sn, Te).

Field emission scanning electron microscopy: FESEM experiments were performed using NOVA NANO SEM 600 (FEI, Germany) operated at 15 KV. $Pb_{0.6}Sn_{0.4}Te$ exhibits the grain size more that 100 μm as can be observed from the field emission scanning electron microscopy image (Figure S5, Supplementary material) measured under back-scattering mode.
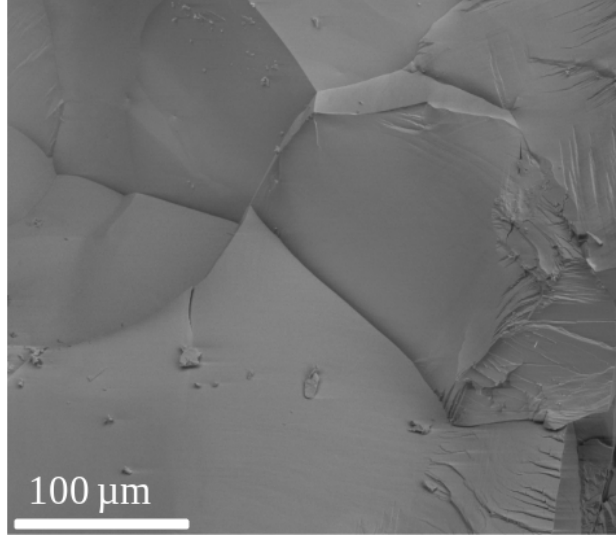

Figure S5: Backscattered mode FESEM image of $Pb_{0.6}Sn_{0.4}Te$ sample showing the grain size bigger than 100 μm.

(IV) <u>Low-temperature measurements:</u> The point-contact spectroscopy measurements were performed in a liquid helium cryostat equipped with a dynamic and a static variabale temperature insert (VTI) that works in a temperature range between 1.4 K and 300 K. The same cryostat is also equipped with a three axis vector magnet where the vertical field (perpendicular to the sample holder disc) is generated by a superconducting solenoid. All the in-field measurements presented in this paper were perfomred by charging the solenoid up to a field of 6 T.

Electrodes of 50 μm gold wire were mounted on $Pb_{0.6}Sn_{0.4}Te$ with silver epoxy (2 component, epotek) and mounted on a disc-shaped sample holder made up of copper. A cernox thermometer and a 50 Ω cartridge heater were directly mounted on the same copper piece for controlling the sample temperature precisely. A Lakeshore temperature controller (Model no. 350) was used to stabilize the temperature with predetermined P, I, D parameters. The point-contacts between the normal metals and the sample were formed by approaching

a sharp metallic tip using a coarse approach mechanism based on a 100 threads per inch (t.p.i.) differential screw purchased from Thorlab.

The dI/dV measurements were done using a SRS 830 lock-in amplifier. The output of the lock-in amplifier was converted to an ac excitation current ($i_{ac}cos\omega t$) that was electronically coupled to a DC current (I_{dc}) generated from a Keithely (model no. 6221) current sourse. The total current $I = I_{dc} + i_{ac}cos\omega t$ was sent through the point-contact. The voltage drop across the point-contact was measured in a pseudo four-probe geometry using a digital multimeter (Keithley: 2000) for the dc component (V) and the same lock-in amplifier as mentioned above (locked at a the frequency ω) for the ac component (v_{ac}). The magnitude of v_{ac} was kept in the range between $10\mu V$ and $50\mu V$. In this limit v_{ac} can be approximated to be proportional to differential change in voltage dV for a given V. The differential change in current dI is measured directly for plotting dI/dV spectra. This technique is traditionally known as lock-in modulation technique for direct measurement of differential conductance.

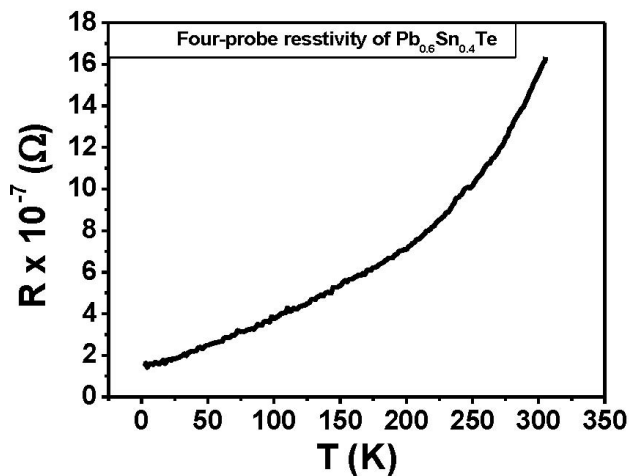(V) <u>Four probe resistivity</u> :

Figure S6: Four-probe resistance vs. Temperature of of $Pb_{0.6}Sn_{0.4}Te$
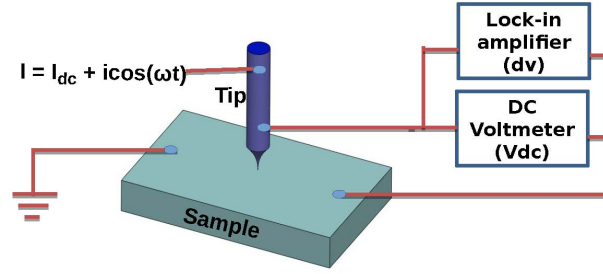
(VI) <u>Spectroscopic measurement</u> :

Figure S7: Schematic diagram of point-contact spectroscopy measurement

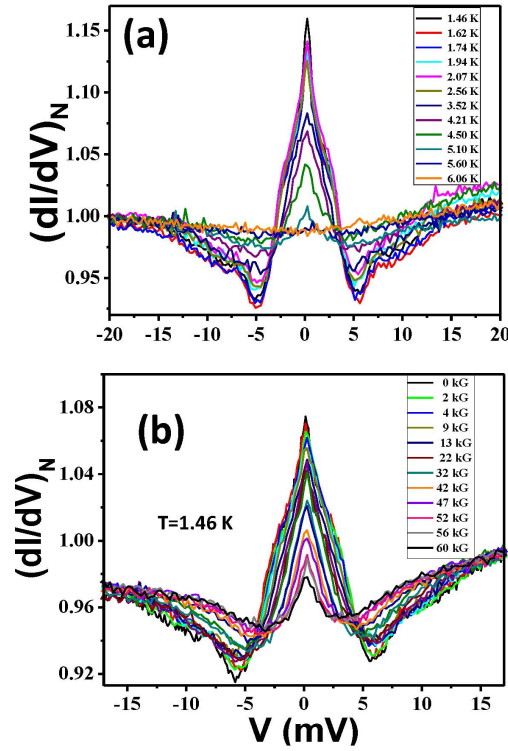(VII) <u>Additional point-contact data with temperature and magnetic field evolution:</u>

Figure S8: **Temperature and magnetic field dependence between Pb$_{0.6}$Sn$_{0.4}$Te and Pd point-contacts:** Evolution of the point-contact spectrum (a) with temperature (2-D plot corresponding to the figure 2(a) of main manuscript) (b) with magnetic field (2-D plot corresponding to the figure 2(b) of main manuscript)
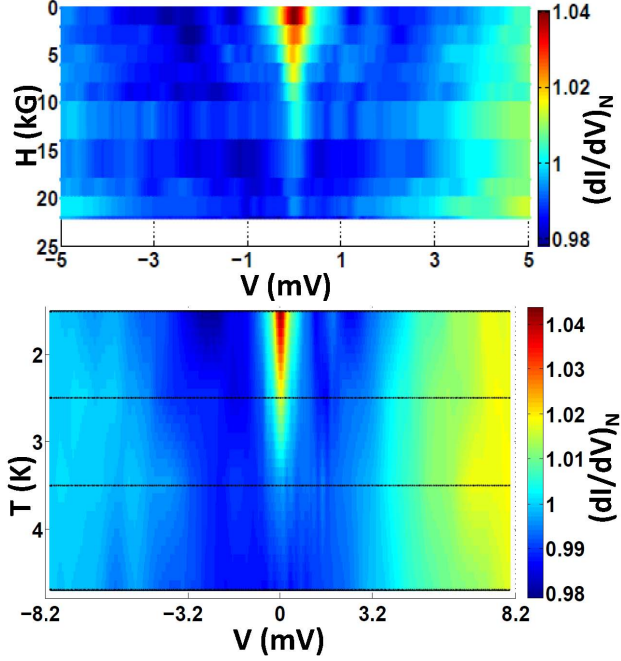
Figure S9: **Temperature and magnetic field dependence between Pb$_{0.6}$Sn$_{0.4}$Te and Ag point-contacts:** Evolution of the point-contact spectrum (a) with magnetic field (b) with temperature.

(VIII) <u>Statistical evaluation of T_c</u> :

With Palladium tip				With Silver tip			
Contact no.	T_c (K)	Normal state resistance (Ω)	Contact diameter (a) in nm	Contact no.	T_c (K)	Normal state resistance (Ω)	Contact diameter (a) in nm
1.	4.2	0.962	123	1.	5.8	1.430	99
2.	5.2	0.274	227	2.	5.0	1.282	105
3.	5.4	0.177	282	3.	5.0	1.255	106
4.	5.4	0.268	229	4.	5.0	1.252	106
5.	6.2	0.468	174	5.	4.5	0.724	140
6.	5.0	0.341	204	6.	4.2	2.046	83
7.	4.5	0.333	206	7.	6.5	1.456	98
8.	4.8	0.312	213	8.	4.5	1.556	95
9.	4.8	0.487	170	9.	5.5	1.420	100
10.	4.8	0.612	152	10.	6.0	1.220	107
11.	4.8	1.350	102	11.	5.0	1.012	118
12.	4.8	1.000	119	12.	6.2	0.864	128
13.	4.8	0.930	123	13.	4.2	0.858	128
14.	4.8	0.744	138	14.	5.0	0.856	128
15.	4.8	2.510	75	15.	4.5	0.736	139
16.	4.8	0.477	172	16.	5.0	4.830	54
17.	5.8	0.323	209	17.	4.2	3.600	62
18.	4.6	0.980	120	18.	3.1	0.611	152
19.	4.9	0.467	174				
20.	3.3	2.210	80				
21.	5.0	6.300	47				
22.	5.9	7.600	43				

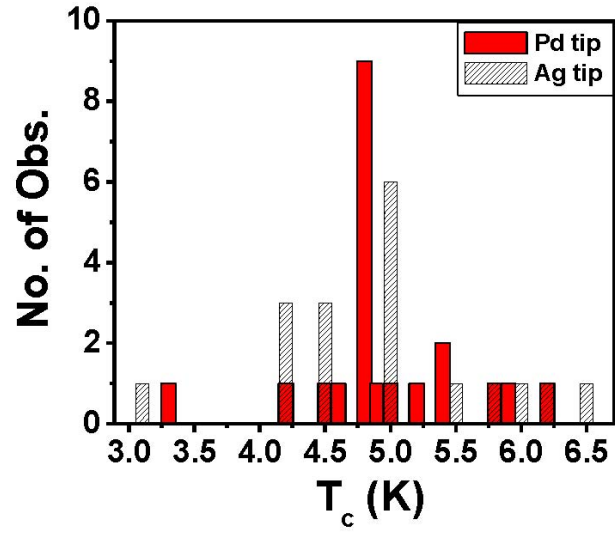Table S1: T_c of different point-contacts with Pd (left)and Ag (right) tips

20

Figure S10: Bar diagram demonstrating T_c at different point-contacts with Pd (red in colour) and Ag (shaded) tips

(VIII) Representative spectra obtained at different points on the sample:
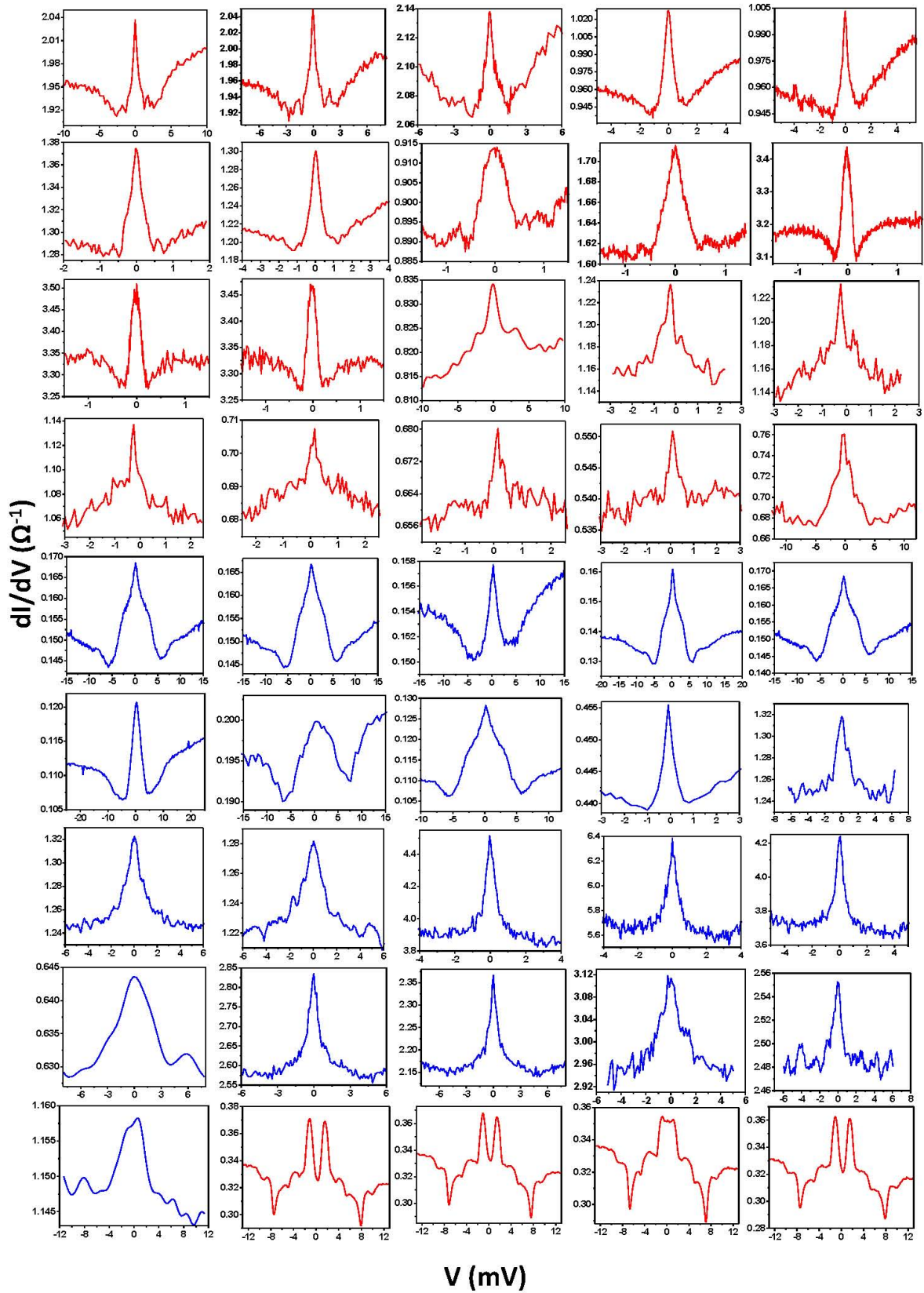
(**Please see the next page**)

Figure S11: dI/dV vs Vdc plots at different point-contacts with Ag (red in color) and Pd (blue in color) tips

22